Article

Theoretical investigation of Responsivity/NEP trade-off in NIR graphene/semiconductor Schottky photodetectors operating at room temperature

Teresa Crisci [1,2], Luigi Moretti [1] and Maurizio Casalino [2]*

[1] Department of Mathematics and Physics, University of Campania "Luigi Vanvitelli", Viale Abramo Lincoln, 5, 81100 Caserta, Italy
[2] Institute of Applied Science and Intelligent Systems “Eduardo Caianiello” (CNR), Via Pietro Castellino, 111, 80131 Naples, Italy
* Correspondence: maurizio.casalino@na.isasi.cnr.it; Tel.: +39-081-6132345 (F.L.)

Abstract: In this work we theoretically investigate the responsivity/noise equivalent power (NEP) trade-off in graphene/semiconductor Schottky photodetectors (PDs) operating in the near-infrared regime and working at room temperature. Our analysis shows as the responsivity/NEP ratio is strongly dependent on the Schottky barrier height (SBH) of the junction and we derive a closed analytical formula for maximizing it. In addition, we theoretically discuss as the SBH is linked to the bias applied to the junction in order to show how these devices could be optimized in practice for different semiconductors. We discover that graphene/n-silicon (Si) Schottky PDs could be optimized at $1550nm$ showing a responsivity and NEP of $133mA/W$ and $500fW/\sqrt{Hz}$, respectively, by a low reverse bias of only $0.66V$. Moreover, we show that graphene/n-germanium (Ge) Schottky PDs optimized in term of responsivity/NEP ratio could be employed at $2000nm$ with a responsivity and NEP of $233mA/W$ and $31pW/\sqrt{Hz}$, respectively. We believe that our insights are of great importance in the field of silicon photonics for the realization of Si-based PDs to be employed in power monitoring, lab-on-chip and environment monitoring applications.

Keywords: graphene; silicon; photodetectors; internal photoemission effect; near-infrared

1. Introduction

Silicon (Si) Schottky photodetectors (PDs) have attracted the interest of the scientific community thanks to the possibility to make Si suitable for detecting the infrared (IR) radiation, that is wavelengths included in the spectrum where Si has a neglectable optical absorption due to its bandgap of $1.12eV$. Schottky Si PDs are metal/Si junctions whose detection mechanism is based on the internal photoemission effect (IPE), i.e., the photo-excitation of charge carriers in the metal and their emission into Si over the Schottky barrier of the junction [1–3]. In other words, in Si Schottky PDs it is the metal, and not the Si, the active material absorbing the incoming optical radiation. In this context, both palladium silicide (Pd_2Si) and platinum silicide (PtSi) Schottky PDs were extensively investigated for the realization of infrared CCD image sensors. Pd_2Si/Si Schottky PDs were developed for satellite applications showing the capability to detect a spectrum ranging from 1 to $2.5\mu m$ if they are cooled to a temperature of $120K$ [4,5]. On the other hand, PtSi/Si Schottky PDs were developed for operating at longer wavelengths ranging from 3 to $5\mu m$ [6,7] even if they require lower temperatures of $80K$. A focal plane array (FPA) constituted by an array of 512×512 PtSi/Si pixels was realized demonstrating first spectacular convergence between Si photonics and electronics [8]. Unfortunately, these devices can only work at cryogenic temperature. Indeed, the low Schottky barrier height (SBH) required to achieve an acceptable efficiency ($0.21eV$ for PtSi [7] and $0.34eV$ for Pd_2Si/Si [4]) is paid in term of PD noise (dark current) which must be reduced by lowering the working temperature. PD noise is typically measured in term of noise equivalent power (NEP), i.e., the minimum detectable optical power, which has a huge impact on both the device sensitivity and the bit error rate (BER) of a communication link. On the other hands, higher Schottky barriers allow achieving low noise but, unfortunately, they also lead to low efficiencies. This

efficiency-noise trade-off is a peculiar characteristic of the Schottky PDs based on IPE.
In 2006 for first time, it was theoretically proposed to use a similar configuration for detecting near-IR (NIR) wavelengths at room temperature [9] taking advantage of interference phenomena on a metal/Si junction incorporated into a high-finesse Fabry-Pèrot microcavity. The main idea was to work with metal/semiconductor junctions characterized by higher SBHs for reducing the dark current and then to recovery the device efficiency by increasing the metal absorption due to the multiple reflections of the optical radiation inside the cavity. Later, many other strategies were pursued for increasing the efficiency of these devices, indeed surface plasmon polaritons (SPPs) [10,11], Si nanoparticles (NPs) [12], metallic antennas [13] and gratings [14], were proposed and investigated. In any case the measured responsivity was lower than $30mA/W$ [12] and $5mA/W$ [15] for waveguide and free-space Schottky PDs, respectively. More important, the efficiency-noise trade-off of these Schottky PDs has never been optimized in term of SBH for achieving high efficiency and low noise at the same time. The low responsivity (i.e., the ratio between the photogenerated current and the incoming optical power) of the Schottky PDs based on metals is mainly due to the low emission probability of the photo-excited carriers from the metal to the Si linked to the momentum mismatch.
Recently, graphene/Si Schottky PDs have shown higher efficiencies with respect to the metallic counterpart and, even if the physical mechanism behind this enhancement is still under debate, it seems linked to the increased emission probability due to the two-dimensionality of the material [16–18]. Although graphene is characterized by a low optical absorption (2.3%) many approaches based on resonant cavity enhanced structures (RCE) [19,20], plasmonic structures [21], waveguiding structures [22] and quantum dots [23] have been proposed for overcoming this drawback. The result is that nowadays graphene/Si PDs [18,22,24] show superior performance with respect to the metallic counterpart representing the most promising solution to the realization of low-cost Si PDs operating in the NIR regime. In addition, graphene offers a novel attractive possibility: The graphene Fermi level, i.e., the SBH with Si, can be simply modified by applying a bias to the junction making feasible the possibility to optimize the efficiency-noise trade-off.
In this work we have theoretically investigated the responsivity/NEP trade-off in graphene/semiconductor Schottky PDs operating at NIR wavelengths and at room temperature. First, we have used the results of the recent literature in order to derive a responsivity/NEP analytical equation for showing how this ratio can be maximized with an appropriate choice of the SBH. Then we have reviewed the SBH dependence on the bias applied to the graphene/semiconductor junctions to show as the responsivity/NEP ratio could be maximized in practice. Finally, we have numerically calculated both responsivity and NEP of graphene/semiconductor PDs discussing their possible applications and highlighting the validity limits of the proposed optimization process. Even if this work has been carried out for gaining more insights on graphene/Si PDs, it is worth mentioning that we trace here a general methodology which can be applied also to different semiconductors as: germanium (Ge), Gallium Arsenide (GaAs) and AlGaAs.

2. Theoretical background

The theory of IPE was first developed by Fowler in 1931 but it was focused on the injection of electrons from a metal into vacuum [25]. Several authors have extended the Fowler's theory to the emission of carriers into semiconductors conceiving the modified Fowler theory [26–28] and providing the following expression for the internal quantum efficiency (IQE) of IPE-based PDs defined as the number of charge carriers N_e produced per absorbed photons N_{ass} [26]:

$$\eta_{\text{int}} = \frac{N_e}{N_{\text{ass}}} = \frac{1}{8E_F} \cdot \frac{(h\nu - q\Phi_B)^2}{h\nu} \tag{1}$$

where E_F represents the Fermi level, $h\nu = hc/\lambda$ is the energy of the incident photon (λ is the wavelength and c the speed of light in a vacuum), q is the electron charge and Φ_B

is the potential barrier at the interface between the metal and the semiconductor. This expression is derived by taking into account the ratio of charge carriers having kinetic energy *normal* to the surface of the junction, necessary to overcome the potential barrier. This mechanism usually leads to low efficiency (about 1%) [29,30], however, it has been demonstrated that two-dimensional materials replacing metals in Schottky junctions enable an enhancement of the IQE [18]. In particular, single layer graphene (SLG) thanks to the presence of π orbitals normal to the semiconductor surface, allows a further higher ratio of conversion of photons in charge carriers. When SLG is used as active medium in a IPE-based PD the (1) can not be longer applied due to its linear band structure in proximity of the Dirac point [31], different density of states (DOS) and probability of emission. However, IQE of Schottky PDs based on SLG has been derived as [18]:

$$\eta_{\text{int}}^{\text{SLG}} = \frac{1}{2} \cdot \frac{(h\nu)^2 - (q\Phi_B)^2}{(h\nu)^2}. \tag{2}$$

The Responsivity R, i.e. the generated photocurrent I_{ph} divided by the incident optical power P_{inc}, provides an estimation of $\eta_{\text{int}}^{\text{SLG}}$ thanks to the following relation:

$$R = \frac{I_{\text{ph}}}{P_{\text{inc}}} = S \cdot \frac{1}{h\nu} \cdot \eta_{\text{int}}^{\text{SLG}} = \frac{S}{2} \cdot \frac{(h\nu)^2 - (q\Phi_B)^2}{(h\nu)^3} \tag{3}$$

where S is the graphene optical absorbance. It is worth mentioning that in (3) the charge carrier q has not been considered in order to express the responsivity in A/W. Graphene has a broadband optical absorption related to the universal fine-structure constant $\alpha = e^2/(\pi\epsilon_0\hbar c)$ [32] and independent of the frequency, $A_G = \pi\alpha \approx 2.3\%$. Here we focus our attention on devices that provide the complete absorption of the incident radiation such as long waveguides and resonant structures, thus we consider $S = 1$.
As the Schottky barrier Φ_B decreases, more electrons can pass into the semiconductor giving rise to an higher responsivity as shown in (2). Unfortunately, also the dark current I_d of the junction increases as Φ_B diminishes due to thermal effect [33]:

$$I_d = A_j A^* T^2 \cdot e^{-\frac{q\Phi_B}{kT}} \tag{4}$$

with A_j area of the Schottky junction, A^* the Richardson constant, T the absolute temperature and k the Boltzmann constant. Furthermore, there is a component of noise intrinsic to the photodetection mechanism: due to the quantized nature of the light, the current is constituted by a succession of random impulses, that cause fluctuations of the measured current (shot noise). The quadratic mean value of the fluctuations linked to both photocurrent I_{ph} and dark current I_d is the following:

$$i_s^2(\Phi_B) = 2qB(I_d(\Phi_B) + I_{\text{ph}}(\Phi_B)) \tag{5}$$

where B is the device bandwidth. In addition to the shot noise, there is a thermal noise (Johnson noise) with quadratic mean value:

$$i_R^2 = \frac{4kTB}{R_L}, \tag{6}$$

being R_L the load resistance of the PD. Since these two noises are statistically independent, their quadratic mean value combine for giving the total noise i_n:

$$i_n = \sqrt{2qB(I_d(\Phi_B) + I_{\text{ph}}(\Phi_B)) + \frac{4kTB}{R_L}}. \tag{7}$$

For applications where a low noise is required the R_L is chosen high enough in such a way the total noise i_n is only limited by the shot noise i_s. At low signal levels $I_{\text{ph}} << I_d$, the condition to make the thermal noise neglectable with respect to the shot noise in (7) is:

$$I_d >> 2V_{\text{th}}/R_L, \tag{8}$$

being the thermal voltage $V_{\text{th}} = kT/q$. At room temperature, condition (8) is mainly depending on both SBH and R_L. Of course, if the thermal noise dominates on the shot noise the total noise i_n doesn't depends on the SBH and the optimization procedure reported here can not be adopted anymore. More than the absolute value of i_n, it is important its magnitude with respect to the generated signal I_{ph} defined as Signal-to-Noise Ratio $SNR = I_{\text{ph}}/i_n$.
In order to find the value of photogenerated current I_{ph} that brings $SNR = 1$, we can take advantage of the definition of the SNR and explicate the expression of i_n through the (7) when condition (8) is fulfilled:

$$SNR = \frac{I_{ph}}{\sqrt{2qB(I_d(\Phi_B) + I_{\text{ph}}(\Phi_B))}} = 1. \tag{9}$$

The square of the previous equation gives a quadratic form in the unknown I_{ph}, by solving it we find:

$$I_{ph} = qB\left(1 \pm \sqrt{1 + \frac{2I_d}{qB}}\right). \tag{10}$$

This expression allows obtaining the incident optical power P_{inc} necessary to get $SNR = 1$ for a PD characterized by a responsivity R. Since the NEP is defined as the incident optical power P_{inc} necessary to get $SNR = 1$ divided by the square root of the bandwidth ($NEP = P_{inc}/\sqrt{B}$), we obtain numerically NEP by considering $B = 1Hz$ in (10) and dividing it by the responsivity R:

$$NEP = \frac{q\left(1 \pm \sqrt{1 + \frac{2I_d}{q}}\right)}{R} \tag{11}$$

which reduces to the very well known formula:

$$NEP \approx \frac{\sqrt{2qI_d}}{R}, \tag{12}$$

being $2I_d/q$ much higher than 1 in typical PDs. It is worth noting that in (12) the sign of R follows the sign of I_{ph} as can be clear by looking at (3).
Optimized PDs are characterized by high responsivity and low NEP. However, by looking at (3) and (12) we understand as by increasing the SBH, the NEP improves at the expense of the responsivity, on the other hand, a SBH decrease is beneficial in term of responsivity but it degradates the NEP. Hence, here we want to investigate the Schottky barrier Φ_B that maximizes the R to NEP ratio. To this aim we introduce a function $G(\Phi_B) = \sqrt{\frac{R}{NEP}}$ by using the (3), (2), (4) and (12):

$$G(\Phi_B) = \sqrt{\frac{R}{NEP}} = \frac{R}{\sqrt[4]{2qI_d}} = C \cdot \frac{(h\nu)^2 - (q\Phi_B)^2}{\sqrt{T}(h\nu)^3} \cdot e^{\frac{q\Phi_B}{4kT}} = C \cdot g(\Phi_B) \tag{13}$$

with $C = 1/(2\sqrt[4]{2qA_jA^*})$ depending on the geometry through the junction area A_j and on the semiconductor through the Richardson constant A^*. Figure 1 (a) displays the behaviour of $g(\Phi_B)$ at $300K$ for three different wavelengths, $1.3\mu m$, $1.55\mu m$ and $2\mu m$, showing the presence of a peak value. From the study of the first and the second derivative of $G(\Phi_B)$ we are able to find the value Φ_B^* of SBH corresponding to this peak:

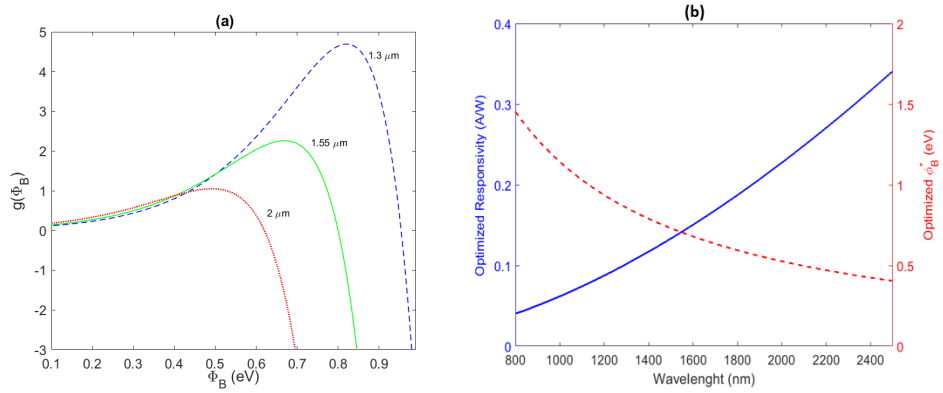

Figure 1. (**a**) Behaviour of $g(\Phi_B)$ at $300K$ for three wavelengths: $1.3\mu m$, $1.55\mu m$ and $2\mu m$; (**b**) optimized responsivity R (blue solid line) and optimized SBH Φ_B^* (red dashed line) as function of the wavelengths.

$\lambda(\mu m)$	$\Phi_B^*(eV)$	$\eta_{\text{int}}^{\text{SLG}}$	$R(A/W)$
1.3	0.86	0.10	0.10
1.55	0.7	0.11	0.14
2	0.52	0.14	0.23

Table 1: Values of the Schottky barrier Φ_B^* optimizing the R/NEP ratio at the three wavelengths of interest: $1.3\mu m$, $1.55\mu m$ and $2\mu m$ at $T = 300K$. The corresponding efficiency $\eta_{\text{int}}^{\text{SLG}}$ and responsivity R, calculated respectively through the (14), (2) and (3), are also shown.

$$\Phi_B^* = -4kT\left[1 - \sqrt{1 + \frac{(h\nu)^2}{16(kT)^2}}\right]. \tag{14}$$

We name Φ_B^* as optimized SBH being the value able to maximize the R to NEP ratio. Figure 1 (b) shows the optimized Schottky barrier Φ_B^* as function of the wavelength. As the wavelength decreases, the Φ_B^* increases, it can be explained by considering that when the wavelength is reduced the photon energy $h\nu$ increases by reducing the responsivity R as shown in (3) requiring a reduction of the NEP to maintain the R/NEP ratio maximized. The NEP reduction can be achieved by an increase of the optimized Φ_B^* reducing the amount of charge carriers able overcome the Schottky barrier due to thermal effects. Even if the Φ_B^* increase produces also a reduction of the responsivity, it is worth reminding that while the NEP is characterized by an exponential decay as function of Φ_B^* ($NEP \sim e^{-\frac{\Phi_B^*}{2V_t}}$), the responsivity is characterized by only a quadratic trend ($R \sim {\Phi_B^*}^2$). Thanks to the equations (3) and (14), it is possible to plot the optimized responsivity in Figure 1 (b), i.e., the responsivity producing the maximized SNR. It is worth highlighting that this optimized responsivity depends only by the SBH of the junction. Figures 1 (b) shows as the optimized responsivity increases by increasing the wavelength due to the decrease in the optimized SBH Φ_B^* giving values at room temperature of $0.10A/W$, $0.14A/W$ and $0.23A/W$ at $1.3\mu m$, $1.55\mu m$ and $2\mu m$, respectively. If higher responsivity are required, of course they can be achieved by lowering the SBH but at the expense of the SNR.

3. Theoretical results and discussion

In this section we theoretically derive as the SBH is linked to the bias applied to the junction in order to show how graphene-based Schottky PDs could be optimized in practice for different semiconductors.

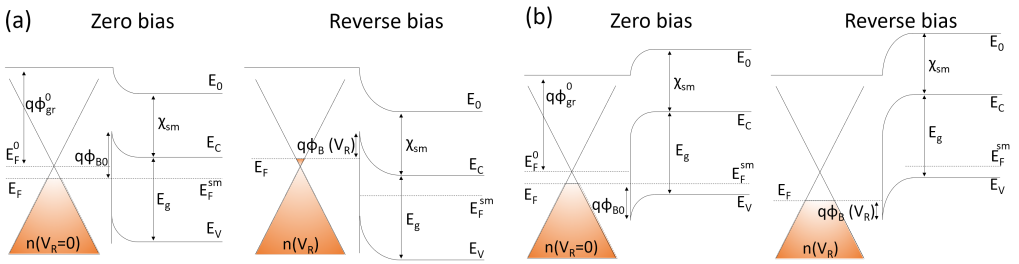

Figure 2. Band diagrams of (**a**) graphene/n-semiconductor and (**b**) graphene/p-semiconductor junctions at the thermal equilibrium and when a reverse bias V_R is applied. At the thermal equilibrium, graphene has an initial carriers density $n(V_R = 0)$. After a reverse bias this charge density becomes $n(V_R)$. E_0 represents the vacuum energy level while E_F^0 is the Dirac point. $\Phi_{\rm gr}^0$, $\chi_{\rm sm}$, E_g, E_C and E_V are, respectively, the intrinsic graphene work function, electron affinity, conduction band, bandgap and valence band. $E_F^{\rm sm}$ is the Fermi energy level in the semiconductor and $q\Phi_{\rm B0}$ the Schottky barrier at zero bias. The values of the Schottky barrier $q\Phi_{\rm B}$ depend on the graphene Fermi energy level E_F that shifts when a voltage is applied.

It's well-known that the SBH Φ_B of the Schottky PDs can be determined by two following equations [33]:

$$q\Phi_B^{(\rm n)}(V_R) = q\Phi_{\rm gr}^0 - \Delta E_{\rm F}(V_R) - q\chi_{\rm sm} \quad \text{(n-type)} \tag{15}$$

$$q\Phi_B^{(\rm p)}(V_R) = E_g - (q\Phi_{\rm gr}^0 - \Delta E_F(V_R) - q\chi_{\rm sm}) \quad \text{(p-type)} \tag{16}$$

(Schottky- Mott relations) where $\chi_{\rm sm}$ and E_g are, respectively, the electron affinity and the bandgap of the semiconductor and $q\Phi_{\rm gr}^0$ is the difference between the vacuum level E_0 and the Dirac point E_F^0 while the graphene Fermi level is E_F. Therefore, $\Delta E_F = E_F - E_F^0$ can be expressed as [34]:

$$\Delta E_F = -sgn(n)\hbar v_F\sqrt{\pi|n|} \tag{17}$$

where $v_F = 1.1 \times 10^8 cm/s$ is the Fermi velocity, $\hbar$ is the reduced Planck constant and n is the carrier density in graphene. The carrier density n is influenced not only by the graphene extrinsic doping n_0 (defined positive and negative for P-type and N-type graphene doping, respectively) but also by the thermal contact with the semiconductor: when a P-doped graphene ($n_0 > 0$) is transferred onto the semiconductor, the space charge $Q_{\rm sm}$ in the depletion region induces an opposite charge $Q_{\rm gr} = -Q_{\rm sm}$ in graphene, creating additional charge carriers and going to alter the carrier density that turns into $n = n_0 + \frac{Q_{\rm gr}}{q}$. The expression of the space charge $Q_{\rm sm}$ when the region is completely depleted is $Q_{\rm sm} = \pm\sqrt{2\epsilon_{\rm sm}NqV_{\rm bi}}$ with $\epsilon_{\rm sm}$ and N, respectively, the dielectric permittivity and the doping density of the semiconductor and $V_{\rm bi}$ the built-in potential. Moreover, the application of a reverse bias allows the electrostatic doping of the graphene: the effect of the voltage adds up to the built-in potential and further changes the charge per unit area in the graphene, $Q_{\rm gr} = \mp\sqrt{2\epsilon_{\rm sm}Nq(V_{\rm bi} + V_R)}$ giving a carrier density:

$$n = n_0 \mp \sqrt{\frac{2\epsilon_{\rm sm}}{q}N(V_{\rm bi} + V_R)} \tag{18}$$

where the signs minus and plus are for N- and P-type semiconductor, respectively. Equation (18) replaced into (17) and then in (15) or (16) gives the desired dependence between the SBH and the reverse bias V_R.

On the other hands, $\Phi_{\rm B0}$ is the SBH at zero bias calculated through the (15) or (16) for $V_R = 0$ (a graphene work function $\Phi_{\rm gr}^0 = 4.6eV$ [35,36], a built-in potential $V_{\rm bi} = 0.6V$, an initial SLG extrinsic p-doping $n_0 = 10^{12} cm^{-2}$ and a semiconductor doping of $N = 10^{16} cm^{-3}$, have been considered). In Table 2 we report the bandgap and the electron affinity of

Semiconductor	$E_g(eV)$	$\chi_{\rm sm}(eV)$	$\Phi_{\rm B0}^{\rm (n)}(eV)$	$\Phi_{\rm B0}^{\rm (p)}(eV)$
Si	1.12	4.00	0.73	0.39
$GaAs$	1.43	4.07	0.66	0.77
$Al_{0.3}Ga_{0.7}As$	1.77	3.77	0.96	0.84
Ge	0.66	4.13	0.60	–

Table 2: Bandgap E_g and electron affinity $\chi_{\rm sm}$ of various semiconductors together with values of SBH when the Schottky junction is formed, calculated thanks to the expressions (15), (16) and (17) by taking into account an initial extrinsic p-doping $n_0 = 10^{12}cm^{-2}$ of the SLG and the thermal equilibrium contact with the substrate. For the calculations we considered low-doped semiconductors, i.e. $N = 10^{16}cm^{-3}$)

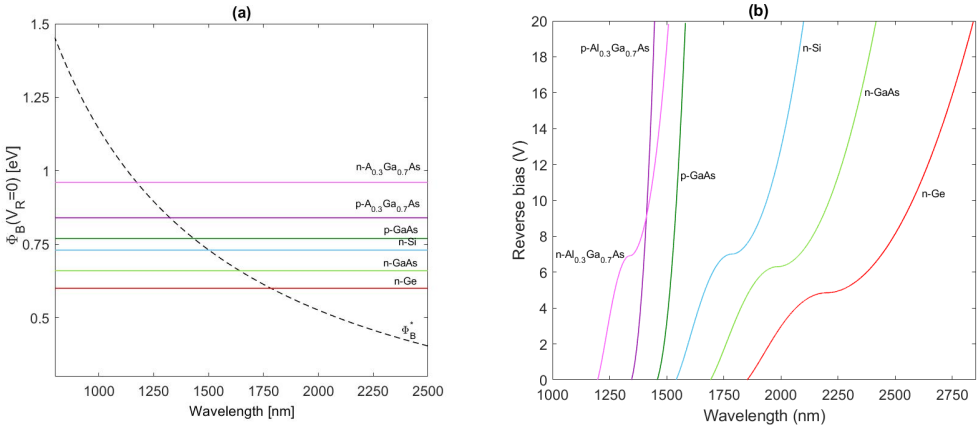

Figure 3. (**a**) Intersection between the curve $\Phi_B^*(\lambda)$ at $300K$ and the values of SBH $\Phi_{\rm B0}$ at the interface between graphene and several semiconductors in conditions of thermal contact (no voltage applied to the junction); (**b**) reverse voltage V_R to apply to the graphene/semiconductor junction as function of the wavelength for maximizing the SNR ratio ($\Phi_B = \Phi_B^*$) for various semiconductors. The values of $\Phi_{\rm B0} = \Phi_{\rm B}(V_R = 0)$ have been calculated through the (15), (16), (17) and (18) by taking into account an initial graphene P-doping of $n_0 = 10^{12}cm^{-2}$ and a doping of $N = 10^{16}cm^{-3}$ for all the semiconductors reported in Table 2.

Semiconductor	$\lambda_{\rm min}(nm)$	$\lambda_{\rm max}(nm)$
$n-Si$	1541	2099
$p-GaAs$	1459	1582
$n-GaAs$	1692	2417
$p-Al_{0.3}Ga_{0.7}As$	1346	1447
$n-Al_{0.3}Ga_{0.7}As$	1197	1508
$n-Ge$	1852	2843

Table 3: Range of wavelengths in which the R/NEP ratio of the Schottky PDs can be maximized by appling a reverse bias up to $20V$.

various semiconductors together with the so-calculated values of Schottky barrier $\Phi_{\rm B0}$ taking into account an initial p-doping $n_0 = 10^{12}cm^{-2}$ for graphene and a low doping of the semiconductors, $N = 10^{16}cm^{-3}$. Figure 3 (a) shows the intersections between these values of SBH $\Phi_{\rm B0}$ for various semiconductors and the curve of the optimized $\Phi_B^*(\lambda)$ at room temperature plotted by (14), suggesting the working wavelength for achieving the highest SNR. On the other hand, for those wavelengths for which $\Phi_{\rm B0} > \Phi_B^*(\lambda)$, the SBH can be lowered down to its optimal value described by (14) by simply applying a reverse bias V_R to the junction. In Figure 3 (b) we plot these values of polarization as function of the wavelength for different semiconductors: it emerges that graphene Schottky PDs based on

p-$Al_{0.3}Ga_{0.7}As$ and p-GaAs can be optimized only in a limited range of wavelengths for $V_R < 20V$ while graphene Schottky PDs based on p-GaAs and n-Si can be optimized at $1.55\mu m$. Interestingly, while n-Si requires only a small reverse voltage of $V_R = 0.66V$ for maximizing its R/NEP ratio at $1.55\mu m$ by a Schottky barrier of $\Phi_B = 0.7eV$, p-GaAs requires an higher reverse voltage of $12V$. Finally graphene/n-Ge Schottky PDs can be optimized at wavelengths longer that $1.55\mu m$. Furthermore, graphene/n-Si PDs can be optimized in term of R/NEP ratio for a large range of wavelengths enabling the possibility to realize bias driven tunable Si PDs. Finally, n-Ge shows the potentialities to be employed for the realization of optimized PDs operating at wavelengths longer than $1.55\mu m$. The range of wavelengths in which the R/NEP ratio can be optimized for various semiconductors, by applying a reverse bias up to $20V$, is summarized in Table 3.

In Figure 4 (a) and (b) we report the values of the quantity of interest in this work, the R/NEP ratio and the optimized NEP, respectively, for all the examined semiconductors by considering a graphene circular area in touch with Si with radius of $500\mu m$ and a PD closed on a load resistance of $10M\Omega$. It is worth reminding that the results shown in Figure 4 are only valid when the condition (8) is fulfilled. In order to verify it, we consider the dark current I_d one order of magnitude higher than $\frac{2V_{\text{th}}}{R_L}$ ($I_d = 10\frac{2V_{\text{th}}}{R_L}$) and we calculate both optimized R/NEP and NEP by the (12). Indeed, the graphene Schottky PDs can be optimized in term of R/NEP ratio at a specific wavelength by the use of semiconductors placed below and above the solid black lines drawn in Figure 4 (a) and (b), respectively. These validity thresholds depend on the load resistance R_L, the SBH Φ_{B} and the graphene area A_j in contact with Si, as clearly shown by the equation (8). We discover that in our case only graphene/n-Si, graphene/n-Ge and graphene/n-GaAs Schottky PDs can be suitable to this optimization procedure. Although Si is typically used for visible detection, this analysis shows that graphene/n-Si Schottky PDs with a maximized R/NEP ratio could be employed for detecting sub-bandgap NIR wavelengths with responsivity and NEP of $133mA/W$ and $500fW/\sqrt{Hz}$ at $1.55\mu m$, respectively. These devices show low NEP enabling their employment for power monitoring and lab-on-chip applications. On the other hand, if the inter-band absorption of Ge is typically used for detecting the wavelength of $1.55\mu m$ for telecommunication applications, the employment of graphene/n-Ge Schottky PDs could allow detection of wavelengths longer than $1.55\mu m$, where the the Ge inter-band absorption suddenly decreases. Indeed, graphene/n-Ge Schottky PDs with optimized R/NEP ration show a responsivity and NEP of $227mA/W$ and $31pW/\sqrt{Hz}$ at $2\mu m$, respectively, enabling their employment in environment monitoring applications. As reported in Figure 4 (b),

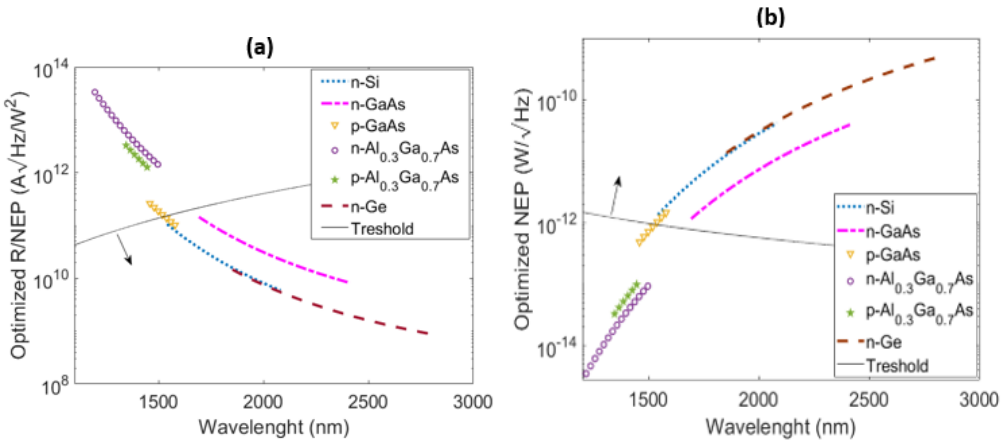

Figure 4. (**a**) the optimized R/NEP and (**b**) the optimized NEP of the Schottky graphene-based PDs for various semiconductors as function of the wavelength range individuated in Table 3. All figures have been obtained at room temperature and by considering a graphene circular area in touch with the semiconductor with radius of $500\mu m$ and a load resistance of $10M\Omega$. The arrows indicate the validity regions of the proposed optimization procedure.

semiconductor as n-Si, n-Ge and n-GaAs can all be employed at room temperature for the realization of optimized graphene-based Schottky PDs in the spectrum ranging from 1955 to 2080nm with a responsivity ranging from 219 to 245mA/W (Figure 1 (b)), however, while n-GaAs would be characterized by a lower NEP, n-Si and n-Ge would have the advantage of a better compatibility with the CMOS technology.

4. Conclusions

In summary, in this work we have theoretically investigated the responsivity/NEP trade-off of NIR graphene/semiconductor Schottky PDs at room temperature. More in detail, we have derived an analytical expression of the SBH able to maximize the R/NEP ratio and we have discussed as the optimized SBH can be tuned by applying a bias to the junction in order to establish the best operation conditions for achieving the higher responsivity as well as the lower noise for various semiconductors. To this aim we have taken into account physics behind the emission of photo-excited charge carriers from graphene to Si, the theory of the graphene/semiconductor Schottky junctions and the property of graphene linked to its two-dimensionality.

Remarkably, we discover that CMOS-compatible materials as Si and Ge could be exploited for the realization of optimized graphene Schottky PDs able to detect wavelengths beyond the limit imposed by their inter-band optical absorption. Indeed, Graphene/n-Si Schottky PDs with maximized responsivity/NEP ratio show responsivity and NEP of 133mA/W and 500$fW/\sqrt{Hz}$, respectively, at 1.55μm by a reverse voltage of only 0.66V. On the other hand, graphene/n-Ge Schottky PDs with maximized responsivity/NEP ratio show the potentialities to work at wavelenghts longer than 1.55μm being for instance characterized by a responsivity and NEP of 227mA/W and 31$pW/\sqrt{Hz}$ at 2μm.

We believe that the insights reported in this work could be of paramount importance in silicon photonics for the realization of optimized PDs to be employed in power monitoring, lab-on-chip and environment monitoring applications.

Conflicts of Interest: The authors declare no conflict of interest.

Abbreviations

The following abbreviations are used in this manuscript:

DOAJ	Directory of open access journals
TLA	Three letter acronym
LD	Linear dichroism

References

1. Casalino, M. Internal photoemission theory: Comments and theoretical limitations on the performance of near-infrared silicon Schottky photodetectors. *IEEE Journal of Quantum Electronics* **2016**, *52*, 1–10.
2. Scales, C.; Berini, P. Thin-film Schottky barrier photodetector models. *IEEE Journal of quantum electronics* **2010**, *46*, 633–643.
3. Crisci, T.; Moretti, L.; Gioffrè, M.; Iodice, M.; Coppola, G.; Casalino, M. Integrated Er/Si Schottky Photodetectors on the end facet of optical waveguides. *Journal of the European Optical Society-Rapid Publications* **2020**, *16*, 1–8.
4. Elabd, H.; Villani, T.; Kosonocky, W. Palladium-silicide Schottky-barrier IR-CCD for SWIR applications at intermediate temperatures. *IEEE Electron Device Letters* **1982**, *3*, 89–90.
5. Elabd, H.; Villani, T.; Tower, J. High density Schottky barrier IRCCD sensors for SWIR applications at intermediate temperature **1982**.
6. Kosonocky, W.; Elabd, H.; Erhardt, H.; Shallcross, F.; Villani, T.; Meray, G.; Cantella, M.; Klein, J.; Roberts, N. 64× 128-Element high-performance PtSi IR-CCD imager sensor. 1981 International Electron Devices Meeting. IEEE, 1981, pp. 702–702.
7. Kosonocky, W.; Elabd, H.; Erhardt, H.; Shallcross, F.; Meray, G.; Villani, T.; Groppe, J.; Miller, R.; Frantz, V.; Cantella, M. Design And Performance Of 64 X 128 Element PtSi Schottky-Barrier Infrared Charge-Coupled Device (IRCCD) Focal Plane Array. Infrared Sensor Technology. International Society for Optics and Photonics, 1982, Vol. 344, pp. 66–77.
8. Wang, W.L.; Winzenread, R.; Nguyen, B.; Murrin, J.J.; Trubiano, R.L. High fill factor 512 x 512 PtSi focal plane array. New Methods in Microscopy and Low Light Imaging. International Society for Optics and Photonics, 1989, Vol. 1161, pp. 79–95.

9. Casalino, M.; Sirleto, L.; Moretti, L.; Della Corte, F.; Rendina, I. Design of a silicon resonant cavity enhanced photodetector based on the internal photoemission effect at 1.55 μm. *Journal of Optics A: Pure and applied optics* **2006**, *8*, 909.
10. Berini, P.; Olivieri, A.; Chen, C. Thin Au surface plasmon waveguide Schottky detectors on p-Si. *Nanotechnology* **2012**, *23*, 444011.
11. Akbari, A.; Tait, R.N.; Berini, P. Surface plasmon waveguide Schottky detector. *Optics express* **2010**, *18*, 8505–8514.
12. Zhu, S.; Chu, H.; Lo, G.; Bai, P.; Kwong, D. Waveguide-integrated near-infrared detector with self-assembled metal silicide nanoparticles embedded in a silicon pn junction. *Applied Physics Letters* **2012**, *100*, 061109.
13. Knight, M.W.; Sobhani, H.; Nordlander, P.; Halas, N.J. Photodetection with active optical antennas. *Science* **2011**, *332*, 702–704.
14. Sobhani, A.; Knight, M.W.; Wang, Y.; Zheng, B.; King, N.S.; Brown, L.V.; Fang, Z.; Nordlander, P.; Halas, N.J. Narrowband photodetection in the near-infrared with a plasmon-induced hot electron device. *Nature communications* **2013**, *4*, 1–6.
15. Desiatov, B.; Goykhman, I.; Mazurski, N.; Shappir, J.; Khurgin, J.B.; Levy, U. Plasmonic enhanced silicon pyramids for internal photoemission Schottky detectors in the near-infrared regime. *Optica* **2015**, *2*, 335–338.
16. Levy, U.; Grajower, M.; Goncalves, P.; Mortensen, N.A.; Khurgin, J.B. Plasmonic silicon Schottky photodetectors: The physics behind graphene enhanced internal photoemission. *Apl Photonics* **2017**, *2*, 026103.
17. Casalino, M.; Russo, R.; Russo, C.; Ciajolo, A.; Di Gennaro, E.; Iodice, M.; Coppola, G. Free-space schottky graphene/silicon photodetectors operating at 2 μm. *ACS Photonics* **2018**, *5*, 4577–4585.
18. Amirmazlaghani, M.; Raissi, F.; Habibpour, O.; Vukusic, J.; Stake, J. Graphene-Si Schottky IR Detector. *IEEE Journal of Quantum Electronics* **2013**, *49*, 589–594. doi:10.1109/JQE.2013.2261472.
19. Casalino, M. Theoretical Investigation of Near-Infrared Fabry–Pérot Microcavity Graphene/Silicon Schottky Photodetectors Based on Double Silicon on Insulator Substrates. *Micromachines* **2020**, *11*, 708.
20. Casalino, M. Design of resonant cavity-enhanced schottky Graphene/silicon photodetectors at 1550 nm. *Journal of Lightwave Technology* **2018**, *36*, 1766–1774.
21. Echtermeyer, T.; Britnell, L.; Jasnos, P.; Lombardo, A.; Gorbachev, R.; Grigorenko, A.; Geim, A.; Ferrari, A.C.; Novoselov, K. Strong plasmonic enhancement of photovoltage in graphene. *Nature communications* **2011**, *2*, 1–5.
22. Goykhman, I.; Sassi, U.; Desiatov, B.; Mazurski, N.; Milana, S.; De Fazio, D.; Eiden, A.; Khurgin, J.; Shappir, J.; Levy, U.; others. On-chip integrated, silicon–graphene plasmonic Schottky photodetector with high responsivity and avalanche photogain. *Nano letters* **2016**, *16*, 3005–3013.
23. Konstantatos, G.; Badioli, M.; Gaudreau, L.; Osmond, J.; Bernechea, M.; De Arquer, F.P.G.; Gatti, F.; Koppens, F.H. Hybrid graphene–quantum dot phototransistors with ultrahigh gain. *Nature nanotechnology* **2012**, *7*, 363–368.
24. Casalino, M.; Sassi, U.; Goykhman, I.; Eiden, A.; Lidorikis, E.; Milana, S.; De Fazio, D.; Tomarchio, F.; Iodice, M.; Coppola, G.; others. Vertically illuminated, resonant cavity enhanced, graphene–silicon Schottky photodetectors. *ACS nano* **2017**, *11*, 10955–10963.
25. Fowler, R.H. The analysis of photoelectric sensitivity curves for clean metals at various temperatures. *Physical review* **1931**, *38*, 45.
26. Elabd, H.; Kosonocky, W.F. PtSi Infrared Schottky-Barrier Detectors With Optical Cavity. *Review* **1982**, *43*, 569.
27. Cohen, J.; Vilms, J.; Archer, R.J. Investigation of semiconductor Schottky barriers for optical detection and cathodic emission. Technical report, HEWLETT-PACKARD CO PALO ALTO CA, 1968.
28. Vickers, V.E. Model of Schottky Barrier Hot-Electron-Mode Photodetection. *Appl. Opt.* **1971**, *10*, 2190–2192. doi:10.1364/AO.10.002190.
29. Raissi, F.; Far, M.M. Highly sensitive PtSi/porous Si Schottky detectors. *IEEE Sensors Journal* **2002**, *2*, 476–481. doi:10.1109/JSEN.2002.806210.
30. Raissi, F. A possible explanation for high quantum efficiency of PtSi/porous Si Schottky detectors. *IEEE Transactions on Electron Devices* **2003**, *50*, 1134–1137. doi:10.1109/TED.2003.812087.
31. Geim, A.; Novoselov, K. The rise of graphene. *Nature Materials* **2007**, *6*, 183–191. doi:10.1038/nmat1849.
32. Nair, R.; Blake, P.; Grigorenko, A.; Novoselov, K.; Booth, T.; Stauber, T.; Peres, N.; Geim, A. Fine structure constant defines visual transparency of graphene. *Science* **2008**, *320*, 1308–1308. doi:10.1126/science.1156965.
33. Sze, S.M.; Ng, K.K. *Physics of semiconductor devices*; John wiley & sons, 2006.
34. Neto, A.C.; Guinea, F.; Peres, N. KS No voselov, and AK Geim. *Rev. Mod. Phys* **2009**, *81*, 109.
35. Yu, Y.J.; Zhao, Y.; Ryu, S.; Brus, L.E.; Kim, K.S.; Kim, P. Tuning the graphene work function by electric field effect. *Nano letters* **2009**, *9*, 3430–3434.
36. Takahashi, T.; Tokailin, H.; Sagawa, T. Angle-resolved ultraviolet photoelectron spectroscopy of the unoccupied band structure of graphite. *Phys. Rev. B* **1985**, *32*, 8317–8324. doi:10.1103/PhysRevB.32.8317.